Mutations in the Putative Pore-Forming Segment Favor Short-Lived Wild-Type Kir2.1 Pore Conformations†

Ruth A. Schwalbe,* Charles S. Wingo, and Shen-Ling Xia

Nephrology Section, Department of Veterans Affairs Medical Center, Division of Nephrology, Hypertension, and Transplantation, University of Florida, Gainesville, Florida 32610

Received June 14, 2002; Revised Manuscript Received July 29, 2002

ABSTRACT: We have characterized single and double mutations in the M1-M2 segment of an inwardly rectifying K^+ channel, Kir2.1, using the cell-attached configuration of the patch-clamp technique. These mutations generated novel N-glycosylation sites at positions 128, 140, 143, and 147. Previously, we showed that these mutants were glycosylated, functional, and at the cell surface, which indicated that the putative pore-forming segment, including the invariant G(Y/F)G sequence of K^+ channels, was extracellular [Schwalbe, R. A., Rudin, A., Xia, S.-L., and Wingo, C. S. (2002) *J. Biol. Chem. 277*, 24382−24389]. In this study, three conductance states, corresponding to the main open state and two subconductance states, were identified in WT Kir2.1 channels expressed in infected Sf9 cells. Kir2.1 channels with mutations in the M1-M2 linker had at least one distinguishable conductance state of WT channels. In addition, these mutations altered the transitions, duration, and frequency of the defined populations of permeating and nonpermeating states. Of note, S128N had permeation rates similar to those of WT Kir2.1, but the total duration of the lower subconductance state was 3−5 times longer. Mutations in the signature sequence, I143N/Y145T, produced channels with permeation rates similar to those of the main open state and lower subconductance state of WT Kir2.1; however, the frequencies of these states were substantially different. These results demonstrate a novel functional role of the M1-M2 segment in regulating the transitions of the Kir2.1 channel and therefore suggest that this segment is a critical structural determinant in adjustments of pore conformations. Additionally, our results indicate that these mutants are correctly folded and thus further substantiate that the M1-M2 segment, including the G(Y/F)G sequence, is topologically extracellular.

Kir2.1, a member of the large gene family of inwardly rectifying K^+ channels (Kir),[1] was cloned from a mouse macrophage cell line (*2*). The inward rectification properties of the expressed Kir channels are voltage- and time-dependent, and these properties of the expressed Kir2.1 channel are virtually identical to those of a native I_{K1} (inward potassium current) channel in the heart (*3*). More recently, ventricular myocytes isolated from Kir2.1 knockout mice were shown to have greatly reduced I_{K1} currents (*4*). Thus, Kirs are essential for maintaining cellular resting membrane potential and in regulating cellular excitability, as well as transepithelial electrolyte transport (*3*).

Kirs are predicted to have two transmembrane segments, M1 and M2, and cytoplasmic N- and C-termini (*2*, *5*). The M1-M2 linker contains the putative pore-forming segment, H5, which has been directly shown to be extracellular (*1*, *6*, *7*). Four identical subunits are proposed to form the functional channel (*8*−*11*), and distinct conformational changes of the subunits lead to channel opening and conduction of ions (*12*−*14*).

Inwardly rectifying K^+ channels open and close spontaneously at membrane potentials negative to the K^+ equilibrium potential (E_K; *15*, *16*). Single channel records show a highly favored open state (main open state) with brief and long closures (*2*, *5*). However, intermediate current levels (subconductances) that are short-lived and much less favorable have been captured (*15*, *17*−*20*). Transitions are mainly between the nonpermeating (closed) state and main current level, and a small amount of the transitions is between the main current and intermediate current levels. In addition, Kir channels have been shown to step from nonpermeating state to intermediate current levels (*15*, *18*, *20*).

Two models have been proposed to explain subconductances, the "partial" closed (single barrel pore) and subunit type (multibarrel pore; *13*, *14*). The partial closed model proposes that each identical subunit contribute to the lining of the pore. The subunit type model predicts that each subunit consists of a conducting pathway, and together they contribute to the single pore. In both models, the highly positive cooperative transition between the nonpermeating state and main open state has been explained by the allosteric interactions between the identical subunits (*12*−*14*). Four subconductance states have been demonstrated for the Kir channel in ventricular myocytes, and a combination of the

† This work was supported by National Institutes of Health Grant DK52990 (to R.A.S.), and with resources and the use of facilities at the Medical Research Service of the Department of Veterans Affairs.

* Corresponding author. Telephone: 352-376-1611 ext 6842. Telefax: 352-379-4048. E-mail: schwara@medicine.ufl.edu.

[1] Abbreviations: Kir, inwardly rectifying K^+ channel; WT, wild type; Kvs, voltage-gated K^+ channels; MES, 2-(*N*-morpholino)ethanesulfonic acid; *I*−*V* plot, current−voltage plot; S1, sublevel 1; S2, sublevel 2; O, fully open state; C, closed state; Sf9, *Spodoptera frugiperda*.

10.1021/bi026304a CCC: $22.00
Published on Web 09/20/2002

two models has been used to describe the subconductances (*13*, *15*). A more recent study reports that Kir2.1 expressed as a naturally occurring channel or in a heterologous system produces a number of subconductances but does not appear to favor the multibarrel pore model (*20*).

Our recent topological studies demonstrate that novel N-glycosylation sites introduced throughout the M1-M2 linker in Kir2.1 (*1*), as well as Kir1.1 (*6*, *7*), could be glycosylated. All glycosylated N-glycosylation substitution mutants expressed whole cell currents that were blocked by barium. We also demonstrated that K^+ selectivity was retained for K117N, S128N, and F147N/C149T of Kir2.1 and M128N, Y144N/F146S, and F146N/F148S of Kir1.1. These studies of Kir2.1 and Kir1.1 indicate that the M1-M2 linker is topologically extracellular, as is the invariant G(Y/F)G sequence. In an attempt to further demonstrate that the single and double mutants were folded correctly, this study was conducted to compare the single channel properties of the Kir2.1 glycosylation substitution mutants to WT Kir2.1 channels. The single channel properties of each of these single and double mutations were evaluated using the cell-attached configuration of the patch-clamp technique. We have identified three nonzero current levels, the main state and two substates, in WT Kir2.1 channels. In addition, our results show that mutations in the M1-M2 linker produce similar size current steps with different frequencies. Therefore, this study demonstrates a novel functional role of the M1-M2 linker, including the putative pore-forming segment, which regulates transitions of the Kir2.1 channel. It also further strengthens that the M1-M2 region is extracellular, because only subtle pore changes were detected in the functional mutant channels.

EXPERIMENTAL PROCEDURES

Molecular Biology. All Kir2.1 cDNAs were constructed using polymerase chain reaction (PCR) and cloned into a baculovirus transfer vector (*1*). Briefly, all constructs contain a FLAG epitope (DYKDDDDK) attached to the 5′ end of mouse Kir2.1 cDNA (GenBank Accession No. XP_122345). In addition, each glycosylation substitution mutant has a novel N-glycosylation site in the M1-M2 linker generated by single or double point mutations. Standard protocols for DNA amplification, isolation, and sequencing were followed (*21*).

Cellular Biology. Cell solutions, cell maintenance, recombinant viruses, and protein expression protocols were carried out as previously described (*1*). In short, insect cells [*Spodoptera frugiperda* (Sf9), American Type Culture Collection] were grown under natural atmosphere at 27 °C in Hink's TNM-FH insect medium (Fisher) containing 10% (v/v) fetal bovine serum (Gibco Life Technologies), 10 μg/mL gentamicin (Sigma Chemical), and 0.1% pluronic F-68 (Gibco Life Technologies), and monolayer cultures were passaged every 3−4 days. Recombinant viruses were generated by cotransfection of Sf9 cells with recombinant baculovirus transfer vectors, encoding WT Kir2.1 and Kir2.1 glycosylation substitution mutant cDNAs and BaculoGold viral DNA (modified AcNPV) as indicated in the manufacturer's booklet (Pharmingen). High viral supernatants were prepared from viral seed stocks (*1*). Infected cells expressing Kir2.1 channel proteins were produced by adding viral supernatant to suspension cultures [cell density, $(1-1.2) \times 10^6$ cells/mL], incubated overnight, and then transferred to 35 mm Petri dishes containing glass coverslips. Cells were also infected by adding viral supernatant (0.5−1 mL) to cells [$(1-2) \times 10^6$ cells] attached to 35 mm dishes containing glass coverslips. Infected cells were incubated at 27 °C for 22−25 h and then transferred to room temperature for patch-clamp analysis up to 72 h.

Single Channel Recordings and Solutions. An Axopatch 200A amplifier with a DigiData 1200 interface (Axon Instruments) connected to a 166 MHz Pentium computer (Millennia; Micron Computer) was used for single channel recordings. All recordings were conducted at room temperature. Fetchex and Clampex software (pClamp 6.0.4; Axon Instruments) was used for data collection. Single channel currents were digitized at 10 kHz, filtered at 1 kHz, and subsequently stored on the computer hard disk.

Patch pipets were pulled from borosilicate capillary glass using a micropipet puller (model P-87, Sutter Instruments) and fire polished using a microforge (MF-83; Narishige International). Fire-polished pipet electrodes had tip resistances between 5 and 12 MΩ. The reference electrode was a Ag/AgCl wire connected to the bath through a salt bridge constructed of a plastic pipet tip filled with 2% agarose (Bio-Rad) in 1 and 0.3 M KCl. The pipet solution contained (in mM) potassium aspartate (140), $MgCl_2$ (5), HEPES (10), EGTA (10), and mannitol (40) (pH adjusted to 7.2 with Tris-OH). The bath solution contained (in mM) potassium aspartate (140), $MgCl_2$ (1), MES (10), and mannitol (60) (pH 6.3, adjusted with Tris-OH). Chemicals used for the electrophysiological experiments were purchased from Sigma Chemical Co.

Data Analysis. Single channel analysis was done on records obtained from patches with seal resistance >10 GΩ. Clampfit, Fetchan, and pSTAT software (pClamp 6.0.4; Axon Instruments) was used for calculating the mean channel current amplitude and all points histograms and estimating opening probability (P_o). The threshold of the current amplitude was manually set to the lower limit of the observed current amplitude. Efforts were made to choose records with a single channel in the patch for determining the P_o of the main current levels. However, in some cases the channel density was high so at least two channels are in the patch (i.e., F147N/F149T). The following formula is used to estimate the P_o:

$$P_o = [\sum(nt_n)/T]/N$$

where N is the number of active nonzero current levels in the patch recording, T is the total recording time, and t_n is the total channel opening time at each current level ($n = 1, ..., N$). The total recording time for P_o estimation at any given potential is at least 60 s or as indicated. When determining the P_o of the fully open state and the substate, two current amplitudes were manually set to the lower limit of each state. In the case where the P_o is low (i.e., Q140N and I143N/Y145T), N might be underestimated, and therefore P_o may be overestimated.

Durations of the substates for WT Kir2.1 and S128N were determined by manually setting the cursors in Clampfit at the beginning and end of each state. In addition, the main current amplitude and substate amplitudes were identified

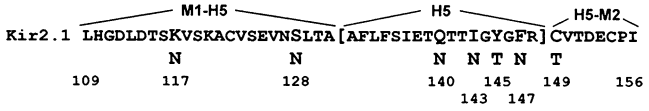

FIGURE 1: Amino acid sequence of the M1-M2 linker of Kir2.1. Letters represent the single amino acid code of the M1-M2 region, which runs from residues 109−156. H5, residues 132−148, is the putative pore-forming segment. Residues 138−146 form the signature sequence and are predicted to confer K^+ selectivity. The M1-H5 linker consists of residues 109−131, and the H5-M2 linker is amino acids 149−156. Enlarged, bold letters in the linear sequence are the amino acids that are mutated to Asn or Thr, as indicated by the single amino acids below the linear sequence. Numbers represent the first and last amino acid residues of the M1-M2 linker sequence, and the residues that were mutated to Asn or Thr.

for each tracing to eliminate error in identifying a substate. The number of channels in analyzed single channel records for WT Kir2.1 was 1−3 and for S128N was 1−2. The records were evaluated prior to and after filtering data at 500 Hz to determine whether there were significant differences produced by filtering. The durations of the substates before filtering and after filtering were similar.

Origin 4.0 (Microcal Software, Northampton, MA) was used for statistical analysis and graphics. The data are reported as means ± SD. Statistical significance was examined using the unpaired Student's *t*-test. A value of $P < 0.05$ was considered significant. The mean current amplitude (*I*) was plotted against the transmembrane potential (applied voltage pulse, *V*) to create a current−voltage relationship (*I*−*V* curve). The unitary conductance was derived from the slope by fitting a linear regression (with confidence of 95%) to the data points in the *I*−*V* curve.

RESULTS

Experimental Development. As we have previously demonstrated, Kir2.1 N-glycosylation substitution mutants S128N, Q140N, I143N/Y145T, and F147N/C149T are glycosylated, are transported to the cell surface, and are functional (*1*). In comparison to WT Kir2.1 channels, all Kir2.1 glycosylation substitution mutants displayed strong inwardly rectifying currents, and whole cell currents were blocked by barium (*1*). As shown in Figure 1, the individual sites were introduced by mutating amino acids 128, 140, 143, and 147 to Asn and residues 145 and 149 to Thr. Since these mutations were made in the putative pore-forming segment, and our former results were unexpected, based on the accepted topological models of K^+ channels, this study was undertaken to determine if these mutations in the M1-M2 linker alter channel opening and permeation. The single channel properties of each of these single and double mutations were evaluated using the cell-attached configuration of the patch-clamp technique.

Main Open Level and Two Intermediate Current Levels of WT Kir2.1 Channels. Single channel tracings of WT Kir2.1 have long openings and both brief and long closures

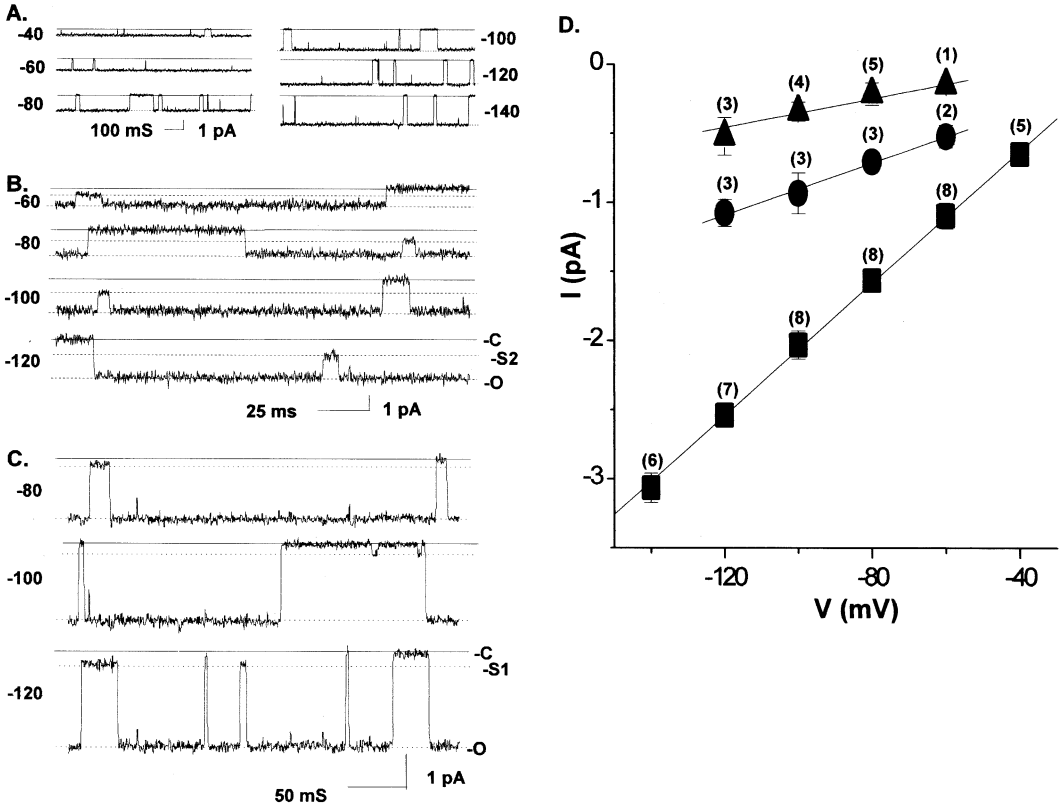

FIGURE 2: Single channel tracings of the main open level and two intermediate current levels of WT Kir2.1. (A) Representative single channel recordings in infected Sf9 cells under the cell-attached configuration. The holding potential for each of the displayed recordings was applied for 10 s. Only 1 s tracings are shown for the sake of clarity. Portions of 1 or 10 s recordings were expanded to demonstrate sublevel 2 (B) and sublevel 1 (C) at the various potentials. Solid lines represent the closed state, and dashed lines denote the fully open state (O), sublevel 2 (S2), and sublevel 1 (S1), as indicated. The potassium concentration in the pipet and bath solutions was 140 mM. (D) Plot of the relationship of the single channel current amplitude and the holding potential. Squares are the main current levels, circles are sublevel 2, and triangles are sublevel 1. The lines represent a least-squares linear regression. The number in parentheses indicates the number of cells.

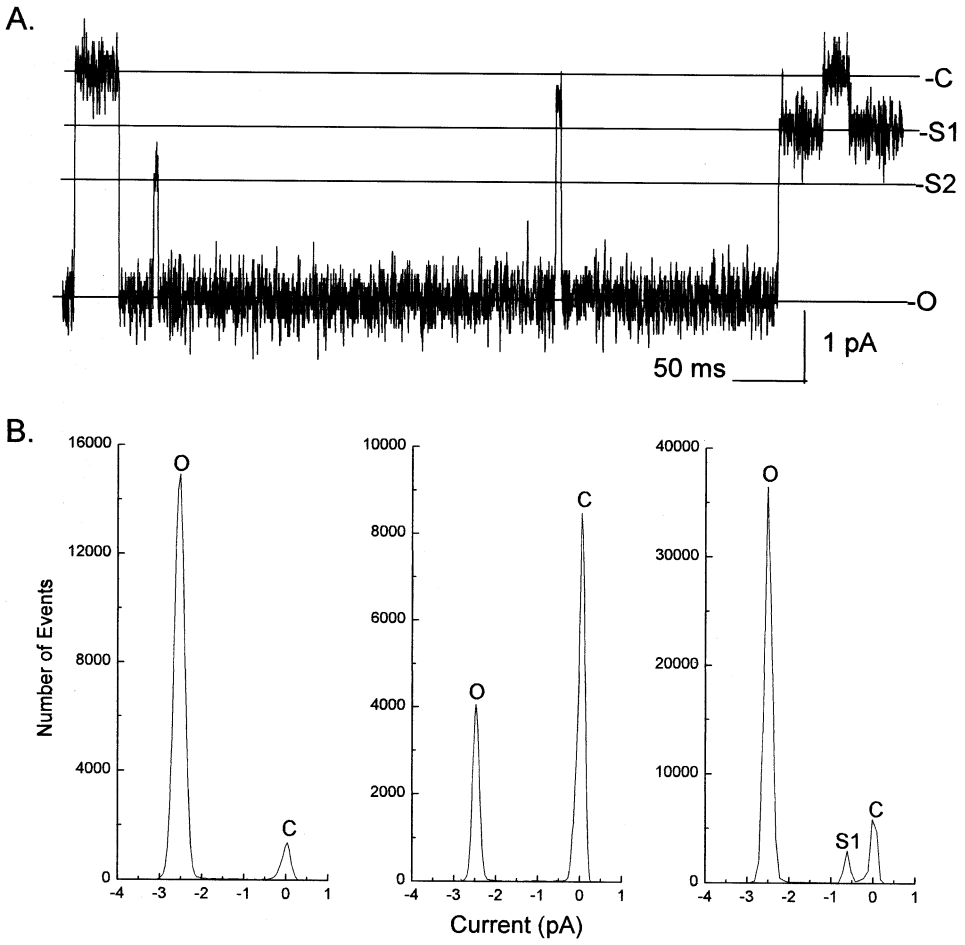

FIGURE 3: Intermediate currents of WT Kir2.1 are observed in the presence of main state activity. (A) Single channel tracing of WT Kir2.1 at a holding potential of −120 mV. The solid line represents the closed state (C). Dotted lines denote sublevel 1 (S1), sublevel 2 (S2), and the fully open state (O). (B) All points histograms from three consecutive 10 s tracings. The histogram on the right includes the trace in panel A. The left and middle panels reveal two peaks, corresponding to the closed state (C) at zero current and the main open state (O), also referred to as the fully open state. The right panel has these two peaks and an additional peak slightly shifted from zero current, which represents sublevel 1 (S1). Only one channel was detected in the patch.

(Figure 2A). The channel appears to switch stochastically between the closed and main open states. However, expansion of the tracings revealed two distinct intermediate current levels at potentials ranging from −60 to −120 mV (Figure 2B,C). The larger intermediate current level called sublevel 2 (S2) was observed following the fully open state of the channel (Figure 2B). Passing from the closed state to this intermediate current level could not be clearly shown because it was very brief and infrequent. The steps of the smaller intermediate current level, referred to as sublevel 1 (S1), were to and from the fully open state (Figure 2C, top and bottom panels) or the closed state (Figure 2C, middle panel). The channel also stepped to sublevel 1 during its transition between closed and fully open states (Figure 3A). Current amplitudes of all three nonzero current levels increased with more negative potentials, and ratios between the step size of the large current step (main current amplitude) and either the larger intermediate current step or smaller intermediate current step were similar at all potentials (Figure 2D). Unitary conductance of the fully open state was 23.9 ± 0.4 pS (n = 8), sublevel 2 was 9.4 ± 0.2 pS (n = 5), and sublevel 1 was 5.2 ± 0.5 pS (n = 6).

The mean P_o of the main current level of WT Kir2.1 was high (mean P_o at −80 mV is 0.82 ± 0.09, n = 6), whereas those of the intermediate current levels were very low. For example, the total duration for sublevel 1 was 794 ms, and sublevel 2 was 342 ms at −120 mV from a total of eleven 10 s recordings that had one to three channels (n = 5).

Three distinct current steps, referred to as a main current level, sublevel 1, and sublevel 2, were clearly observed in WT Kir2.1 channels, but the subconductance states were rare (Figure 3A). For instance, all points histograms of 10 s tracings usually reported two peaks, corresponding to the closed and main open states (Figure 3B, left and middle panels). However, a 10 s tracing that followed the previous two records and includes the trace in Figure 3A, clearly shows an additional peak, which corresponds to sublevel 1 (Figure 3B, right panel). The openings of both states were not simultaneous, indicating that these two nonzero current amplitudes are from the same channel. Sublevel 2 could not be observed in a similar manner because the duration of the event was brief (Figures 2B and 3A).

Mean Current Amplitudes of the M1-M2 Linker Mutants Are Similar to Those of WT Kir2.1. The three mean current amplitudes at −120 mV of WT Kir2.1 were defined as the main open current level, sublevel 2, and sublevel 1, and the M1-M2 mutants had at least one of these three distinct current levels as shown in Figure 4. S128N, similar to WT channels, expressed all three nonzero current levels. The fully open current level and sublevel 1 were detected in I143N/

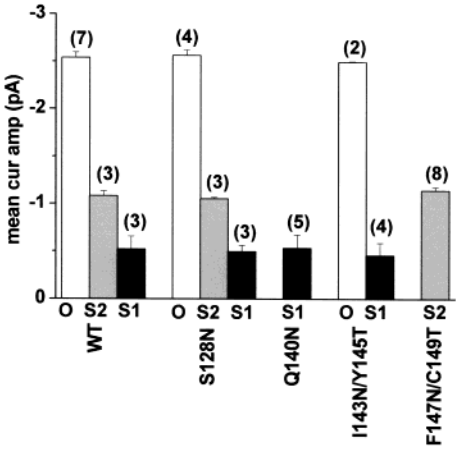

FIGURE 4: Three distinct current levels of WT Kir2.1 are compared to the current levels of the Kir2.1 mutants. The mean current amplitudes of the fully open state (O), sublevel 1 (S1), and sublevel 2 (S2) of WT Kir2.1 and the N-glycosylation mutant channels at −120 mV. The mean current amplitudes were −2.54 ± 0.06 pA (O), −1.08 ± 0.05 pA (S2), and −0.61 ± 0.14 pA (S1) for WT Kir2.1, −2.56 ± 0.06 pA (O), −1.05 ± 0.02 pA (S2), and −0.50 ± 0.07 pA (S1) for S128N, −0.53 ± 0.14 pA (S1) for Q140N, −2.50 ± 0.01 pA (O) and −0.46 ± 0.13 pA (S1) for I143N/Y145T, and 1.14 ± 0.04 pA (S2) for F147N/C149T. The number in parentheses represents the number of cells used to determine the mean current amplitudes.

Y145T mutant channels. Of interest, observation of the fully open level in the presence of sublevel 1 indicates that the two mutations in the signature sequence of K^+ channels do not reduce current amplitudes of the fully open state. Current amplitudes in Q140N and F147N/C149T were similar to sublevel 1 and sublevel 2, respectively. In both cases, the fully open state was not detected, suggesting that these reductions in current amplitudes are due to destabilization of the fully open state and stabilization of WT Kir2.1 substates or a result of reduction in the current amplitude of the fully open state. We also observed current amplitudes such as sublevel 1 at −80 mV for F147N/C149T as shown below. Thus, mutations of Kir2.1 in the M1-M2 linker produce channels with similar current amplitudes as those in the WT channel, and the following sections will show additional details to support these three defined permeation rates of the Kir2.1 channel.

Mutation of Ser128 to Asn in the M1-H5 Linker Alters Spontaneous Single Channel Gating. Single channel records of three distinct nonzero current levels, similar to WT Kir2.1, and the $I-V$ relationships for these current levels of S128N are shown in Figure 5. In contrast to WT Kir2.1 channels, transitions between sublevel 2 and either the main open state or closed state could be shown (Figure 5B). Similar to WT Kir2.1, sublevel 1 could pass to the closed or open states and visa versa (Figure 5C). Current−voltage relationships were derived for the main open level, sublevel 2, and sublevel 1. The inward conductance of the main current level was 24.3 ± 0.5 pS ($n = 5$), sublevel 2 was 9.3 ± 0.4 pS ($n = 3$), and sublevel 1 was 6.4 ± 0.5 pS ($n = 3$; Figure 5D). The ratios between the current amplitudes of the main state and sublevel 2 were similar at all potentials, as were those for sublevel 1.

The P_o of the main open state was high (mean P_o was 0.77 ± 0.16 at −80 mV, $n = 3$) and was much lower for the sublevels. From a total recording time of 195 s, the total duration of sublevel 1 was 3576 ms, and that of sublevel 2 was 340 ms at −120 mV ($n = 3$, one to two channels). In comparison to WT Kir2.1 channels, the estimated ratio of

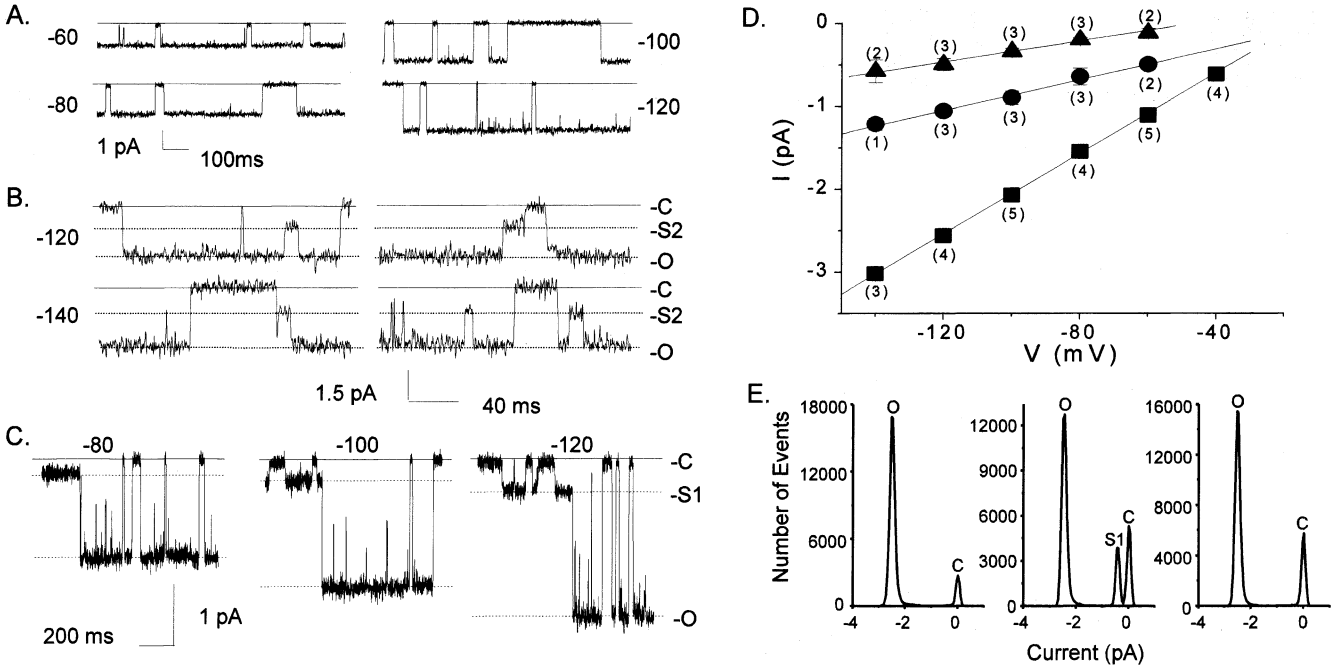

FIGURE 5: Fully open state and two short-lived subconductance states detected in S128N channels. (A) Representative single channel tracings of the main current amplitude at the various potentials. (B and C) Selected and expanded regions of single channel tracings at the various pulses to demonstrate sublevel 2 (S2) and sublevel 1 (S1), respectively. The solid line indicates the closed state. The dashed line denotes the main and intermediate current levels. (D) Mean current amplitudes of the main open state and the intermediate current levels plotted at the indicated potentials. The squares represent the main current amplitude, circles are S2, and triangles are S1. The number in parentheses is *n*. (E) All points histograms from three consecutive tracings. The left and right panels detect two peaks, representing the closed state (C) as zero current and the main open state (O), also referred to as the fully open state. The middle panel reveals an additional peak slightly shifted from the zero current, which corresponds to sublevel 1 (S1). Only one channel was detected in the patch.

the total duration of sublevel 1 for WT Kir2.1 to the total duration of sublevel 1 for S128N was about 1:3−5, and the estimated duration ratio of sublevel 2 was about 1:1. These ratios indicate that sublevel 1 is more prevalent in S128N channels than WT Kir2.1, and that of sublevel 2 is comparable.

Similar to WT Kir2.1, all points histograms of 10 s tracings of S128N usually showed two peaks, but a third peak, corresponding to sublevel 1, was also clearly observed (Figure 5E). Furthermore, the openings of the two distinct states do not overlap. These results indicate that mutating Ser128 to Asn increases the total duration of sublevel 1 and also appears to alter the transition from the closed to the main open state by entering a more stable sublevel 2.

Mutations in the Signature Sequence Modify Channel Opening and Permeation. Single channel records of I143N/Y145T reveal two distinct nonzero current levels (Figure 6A,B). The resultant slope conductance was 23.6 ± 0.5 pS (n = 4; O) and 6.7 ± 0.3 pS (n = 5; S1; Figure 6C). Both of these permeation rates were detected in WT Kir2.1 and S128N channels. However, the main current level was the smaller conducting state, and the minor current level was the highly favored open state of WT Kir2.1. The transition between the fully open and closed states usually involved a visit at sublevel 1 (Figure 6A).

The mean P_o of sublevel 1 was 0.09 ± 0.05 (n = 3). Fully open levels were rare compared to sublevel 1, and when the current went above sublevel 1, the channel usually flickered too much to get an accurate measurement of the current amplitude. From one cell expressing I143N/Y145T channels the recording was very stable, and it appeared that the opening to the full level was voltage-dependent. For example, one channel opening event was observed every 120, 70, 16, 15, and 7 s at −80, −100, −120, −140, and −160 mV, respectively. In addition, the duration of the opening at more negative potentials appeared to be longer (Figure 6A).

The main current level observed in Q140N channels was sublevel 1 (Figure 7A), similar to I143N/Y145T. The mean inward conductance was 5.4 ± 0.3 pS (n = 7; Figure 7B). At some time intervals the current levels would rise above sublevel 1 and display channel flickering so current levels above sublevel 1 could not be categorized. Figure 7C shows a representative 5 s tracing of Q140N. The openings are short and few, while the closures are long. The P_o for Q140N was 0.09 ± 0.05 (n = 5). Similar long single channel records were observed for I143N/Y145T. The only difference between the two mutant channels is that the fully open state was observed to be stable for brief periods in I143N/Y145. Thus, mutations in the signature sequence appear to disrupt the transition between the highly favored open state and closed state of WT Kir2.1 channels, not reduce current amplitudes of the main current levels of WT Kir2.1.

H5 Mutations Alter Channel Gating and Permeation. Mutations of Phe147 to Asn and Cys149 to Thr of Kir2.1 produce a main current level that is less than the main open level for WT channels (Figure 8). This main current level is similar to sublevel 2 detected in WT Kir2.1 (Figure 2B) and S128N (Figure 5B), as is the resultant slope conductance (9.2 ± 0.7 pS; n = 8; F147N/C149T). Because current amplitudes and unitary conductance of F147N/C149T are similar to sublevel 2 of WT Kir2.1 and S128N, we refer to the main current amplitude as sublevel 2. Interestingly, single

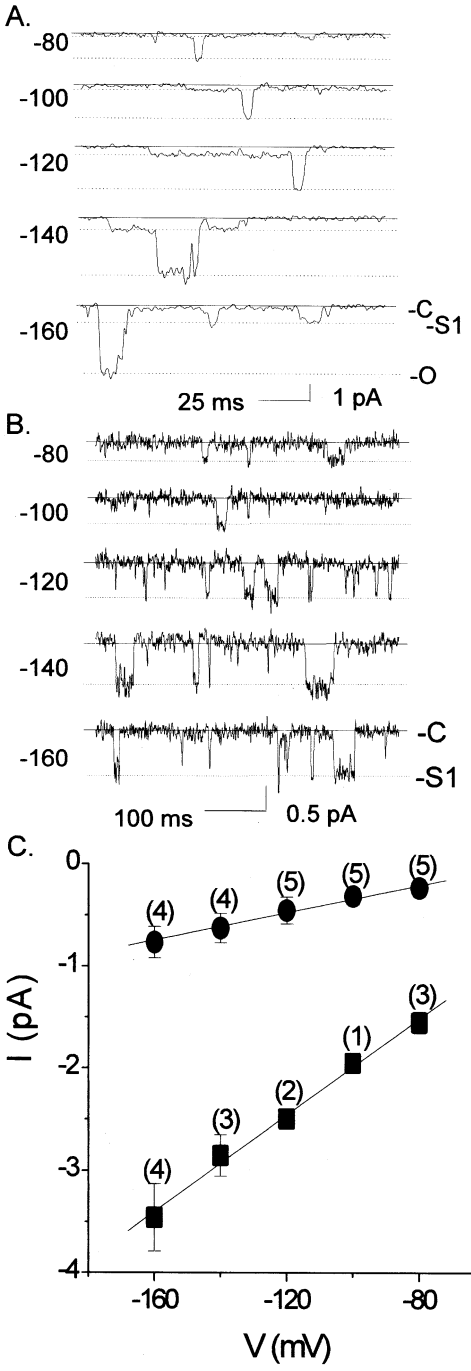

FIGURE 6: Single channel current levels identified in I143N/Y145T mutant channels. (A and B) Selected and enlarged portions of single channel records at the different potentials to illustrate the fully open state and intermediate current level (S1). (C) Current−voltage relation of single channel activity constructed from the number of cells as indicated by the number in parentheses above each point. Squares are current amplitudes of the fully open state, and circles are S1.

channel recordings of F147N/C149T have long openings and brief and a few long closures (Figure 8C), similar to the main current level of WT channels, and thus the mean P_o of the main current level was high (0.91 ± 0.09; n = 3).

Overall, sublevel 2 was highly favored and only short-lived smaller current levels were observed. However, one cell displayed a long-lived smaller current step (Figure 9), which appeared to be similar to the short-lived smaller current steps. The mean current amplitude of this smaller

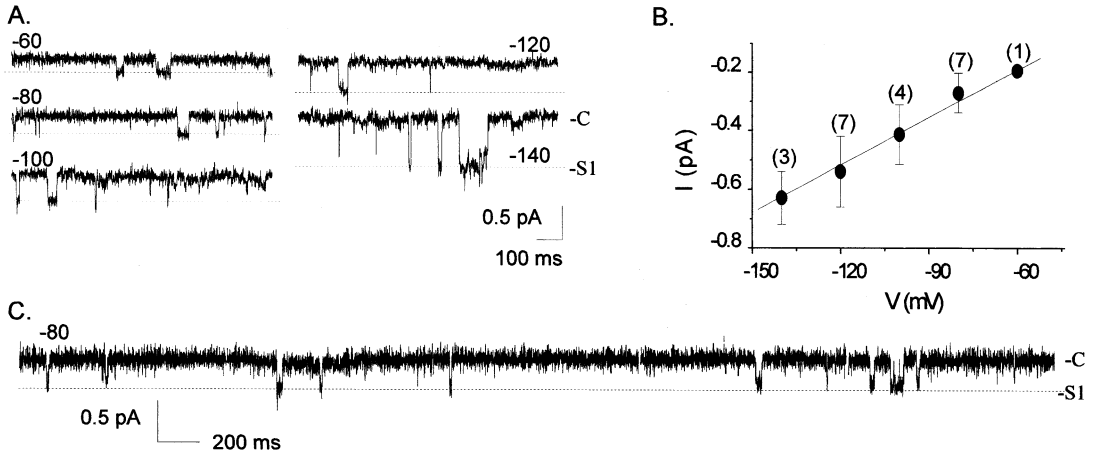

FIGURE 7: Q140N mutant channels expressed intermediate current levels. (A) Representative single channel records at different potentials. (B) Current−voltage relationship of the Q140N mutant channel. (C) Representative 5 s single channel trace at −80 mV. C represents the closed state, and S1 indicates sublevel 1.

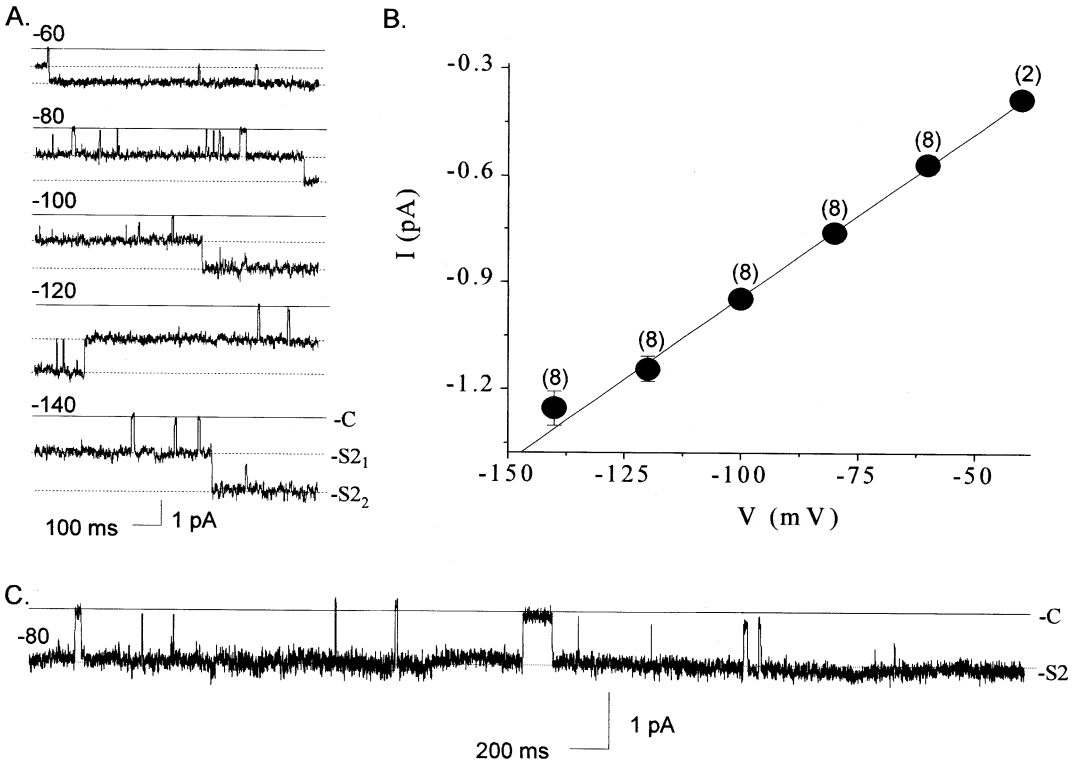

FIGURE 8: An intermediate current level detected in F147N/C149T mutant channels. (A) Representative single channel traces at several potentials. (B) Current−voltage plot of the main current level. (C) A representative 5 s single channel tracing at −80 mV. C is the closed state, S2 is sublevel 2, $S2_1$ is the opening of one channel to this level, and $S2_2$ indicates two channels.

current level was 0.33 ± 0.04 pA ($n = 1$) at −80 mV. Since this current amplitude was similar to sublevel 1 of WT Kir2.1, S128N, Q140N, and I143N/Y145T, we refer to it as sublevel 1. Transitions were between both closed state and sublevel 1 and between sublevel 1 and sublevel 2. The P_o of sublevel 1 and sublevel 2 for F147N/C149T from four consecutive 10 s pulses, individually and total time, at −80 mV was 0.01 ± 0.03, 0.90 ± 0.28; 0.01 ± 0.01, 0.97 ± 0.14; 0.14 ± 0.22, 0.66 ± 0.46; 0.01 ± 0.02, 0.95 ± 0.17; and 0.04 ± 0.07, 0.87 ± 0.14, respectively. It appears that sublevel 1 (0.14 ± 0.22) is more stable when sublevel 2 (0.66 ± 0.46) is less stable. Thus, overall the P_o and frequency of this smaller current level in F147N/C149T channels were very low, but these results provide evidence for the existence of sublevel 1 in F147NC149T channels, as observed in WT, S128N, Q140N, and I143N/Y145T, and that sublevel 1 can step to sublevel 2.

DISCUSSION

Three distinct conductance states were identified in WT Kir2.1 channels expressed in infected Sf9 cells (Table 1). The main current level referred to as the fully open state of WT Kir2.1 channels was long lasting. This result is consistent with observations made from Kir2.1 channels expressed in other cell lines (*2*, *17*). The two intermediate current levels were relatively short lasting under our experimental conditions. These intermediate current levels were observed in the presence of main state activity, interconverted with the main state, and the openings did not overlap, indicating two distinguishable subconductance states (*13*). Current levels

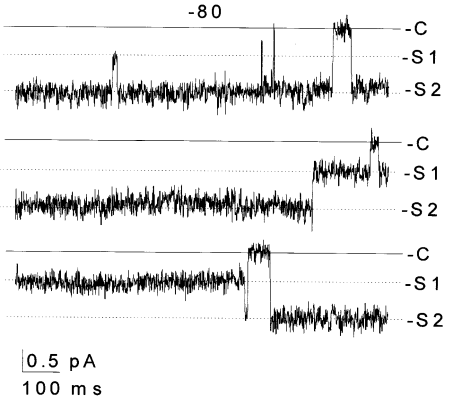

FIGURE 9: Sublevel 1 detected in F147N/C149T mutant channels. Representative single channel tracings at −80 mV. C represents the nonpermeating state, S1 refers to sublevel 1, and S2 refers to sublevel 2.

of subconductance 1 and subconductance 2 were 23% and 39% of the main current level, respectively. Similar subconductance states (25% and 46% of the main conductance) of a Kir channel in ventricular cells were reported by Sakmann and Trube (*15*). Thus, WT Kir2.1 channels expressed in infected Sf9 cells have at least two subconductance states.

Recently, Picone et al. (*20*) have shown that WT Kir2.1 expressed in *Xenopus* oocytes produces channels with a large range of unitary conductances (*20*). In particular, they have characterized two Kir2.1 channels, called the large and small channels, and suggested that they are part of a channel complex. The current amplitudes of these two Kir2.1 channels appear to be similar to the main open state and sublevel 1 in this study. The all points histogram from our study does not show the open times of these two nonzero current levels overlapping for WT Kir2.1 (Figure 3B), as well as S128N (Figure 5E). Single channel tracings of WT and S128N show that some of the transitions between the closed and open state involve a visit to sublevel 1 or 2 (Figures 3A and 5B,C). Our results also show that the sublevel 1 opening from either the closed state or main open state can be quite long (Figures 2C and 3A). Therefore, we interpret the current amplitude referred to sublevel 1 as a subconductance state of Kir2.1.

However, our study does not rule out that small and large Kir2.1 channels were present in a channel complex as demonstrated by Picone et al. (*20*) because these two states could be detected opening simultaneously when two or more main openings were detected in a patch. In addition, sublevel 1 was observed in the absence of the main open level for quite long periods. Thus, it is possible that under certain conditions different permeation rates of Kir2.1 may be favored and, furthermore, that Kir2.1 channels with different permeation rates make up a channel complex of small and large channels, as well as intermediate channels. Future studies are needed to determine whether specific protein modifications can favor different permeation rates and also to determine if a channel complex is composed of channels with different permeation rates that correspond to the main open current level and intermediate current levels of the Kir2.1 channel. Nonetheless, our results do support that Kir2.1 expressed in Sf9 cells has three permeation rates, a fully open state (main current level) and two subconductance states (intermediate current levels).

All three permeation rates of the WT Kir2.1 channel were observed when Ser128, a residue preceding the putative pore-forming segment (Figure 1), was substituted with Asn (Table 1). When mutations I143N/Y145T and Q140N were introduced in the signature sequence of K^+ channels, the single channel records revealed two current levels. These current amplitudes were similar to those observed in WT Kir2.1 and S128N channels and therefore indicate that the two current levels for I143N/Y145T are the fully open state and sublevel 1 of WT Kir2.1 and S128N, and that of Q140N is sublevel 1. Of note, observation of the fully open state for I143N/Y145T indicates that sublevel 1 is not a reduction in the fully open state of WT Kir2.1 but similar to sublevel 1 of WT Kir2.1 and S128N channels. In the case of Q140N the fully open state was not detected so it is possible that this mutation reduces the current amplitude of the fully open state. However, our results highly favor that the main current amplitude of Q140N is sublevel 1 because the current amplitudes are similar to WT Kir2.1, S128N, and I143N/Y145T. In addition, the P_o's of Q140N and I143N/Y145T are similar. As shown in Figures 6 and 7, the single channel tracings of I143N/Y145T and Q140N are identical, except for the rare opening to the fully open state for I143N/Y145T. Other mutations in the putative pore-forming segment, F147N/C149T, produced two current levels that were less than the main open state of WT Kir2.1 channels. The larger current amplitude was similar to sublevel 2 of WT Kir2.1 and S128N, and the smaller current amplitude was similar to sublevel 1 of WT Kir2.1, S128N, Q140N, and I143N/Y145T, suggesting that only the intermediate permeation rates are present in F147N/C149T channels. An alternative interpretation is that the larger intermediate current level is similar to the fully open state of WT Kir2.1 with reduced current amplitudes, because the P_o was high like WT Kir2.1. On the other hand, the single channel tracings of the lower intermediate current appear to be more like sublevel 1 than sublevel 2. This would mean that the mutations changed the permeation rate of the fully open state and maintained that

Table 1: Conductance States and Transitions of Kir2.1 Channels[a]

Kir2.1	O	S2	S1	C ⇄ O	O ⇄ S2	O ⇄ S1	C ⇄ S2	C ⇄ S1	S2 ⇄ S1	$P_{o(main)}$
WT	+	+	+	+	+	+	−	+	−	high
S128N	+	+	+	+	+	+	+	+	−	high
Q140N	−	−	+	−	−	−	−	+	−	low
I143N/Y145T	+	−	+	+	−	+	−	+	−	low
F147N/C149T	−	+	+	−	−	−	+	+	+	high

[a] The three distinct current levels of the Kir2.1 channels are categorized into three permeating states: the fully open state (O), sublevel 2 (S2), and sublevel 1 (S1), respectively. The two antiparallel arrows between two states indicate transitions between the respective states. The mean opening probability of the main state for each channel is indicated by $P_{o(main)}$. A plus sign means the permeating state or transition could be demonstrated, and a minus sign indicates that they were not.

of sublevel 1. These results demonstrate that WT Kir2.1 channels consist of at least three specific conductance states, a fully open state and two subconductance states, and that these mutants with N-glycosylation sites introduced in the M1-M2 linker retained at least one WT-like conductance state.

Differences between WT Kir2.1 and the mutants are evident when comparing the transition, duration, and frequency of the three conducting states (Table 1). For WT Kir2.1, the transitions were between the intermediate current levels (sublevel 1 and 2) and the main state. The lower current step (sublevel 1) was also to or from the closed state. Similar transitions were observed in S128N. In addition, the larger intermediate current step (sublevel 2) could be demonstrated to occur from or to a nonpermeating state (Figure 5B). This transition was observed in WT Kir2.1 but could not be clearly shown because the duration of sublevel 2 was only about 1 ms. A clear difference between S128N and WT Kir2.1 was that the total duration of sublevel 1 was longer for S128N than WT Kir2.1. Significant differences were also present in Kir2.1 channels with mutations in the putative pore-forming segment. The main current level in I143N/Y145T mutant channels was sublevel 1, while the minor current level was the fully open state of WT Kir2.1. Transitions between these two conducting states and the nonconducting state were similar to WT Kir2.1. Q140N was similar to I143N/Y145T but did not step to the fully open state. Sublevel 2 could not be demonstrated in Q140N or I143N/Y145T. The transitions between the two current levels of F147N/C149T were between the closed and open states as well as each other. As mentioned, the current amplitudes suggest that the current levels are sublevel 2 (main current level) and sublevel 1 (minor current level), and therefore our interpretation is that the transitions were between sublevel 2 and closed state, sublevel 1 and closed state, and between sublevels. The frequency of sublevel 2 was very high, whereas that of sublevel 1 was rare and none for the fully open state. These results provide direct evidence that mutations in the M1-M2 linker of Kir2.1 channels alter the transition, duration, and frequency of these three distinct populations. Furthermore, the results indicate that mutations in this region produce slight changes in the pore, which result in stabilizing minor WT pore conformations.

Single channel behavior of WT Kir2.1 was dominated by two states, the closed and main open states; however, Kir2.1 channels with mutations in H5 were dominated by intermediate current levels that were identified as the two subconductance states of WT Kir2.1 channels. The predominant states of S128N channels were the closed and main open states, but unlike WT Kir2.1, the duration of sublevel 1 was longer, and also the transition between the closed and main open states could be shown to involve a short intermission at sublevel 2 (Figure 5B). If ion permeation rate increases with the number of subunits in the open conformation as described by single pore (partial closed) and multipore (subunit type) models (*13*, *14*), then these introduced mutations reduce the number of subunits in the open conformation. The "partial closed" model would also include different conformational states of the oligomeric pore, including the closed state, main open state, and each minor open state (*13*). Nonetheless, the models would agree that the closed and main open pore conformations of WT Kir2.1 are highly favorable whereas the intermediate pore conformations (subconductance states) are unfavorable, and thus the transition between the closed state and main open state has a strongly positive cooperativity. Mutations S128N, Q140N, I143N/Y145S, and F147N/C149T in the M1-M2 linker give rise to Kir2.1 channels that favor various intermediate pore conformations to a larger extent than WT Kir2.1 channels. Taken together, these results suggest that subtle changes of the pore produced by these mutations reduce the positive cooperativity of this transition.

The M1-M2 linker mutants favored intermediate pore conformations to a greater extent than WT Kir2.1. These findings support that this segment alters pore conformations of the homomultimer channel. In addition, H5 and H5-M2 appear to be directly involved because Koster et al. (*22*) have shown that multimeric structures of Kir1.1 containing H5, H5-M2, M2, and C-terminal regions were coimmunoprecipitated to a larger extent than those without these regions (*22*). Other functional studies have also shown that conformational changes in the M1-M2 linker alter channel gating and permeation. For example, utilization of the native N-glycosylation site, as well as other introduced sites throughout the M1-M2 linker, was shown to stabilize the open state of the channel (*23*). This would indicate that glycosylated Kir1.1 favors a different conformational structure than its unglycosylated counterpart. In addition, ion permeation was shown to be modulated by M1-H5 and M2-H5 regions in Kir 6.0 channels and thus control the conformation of the permeation pathway (*24*). Distinct subconductance levels were introduced when the backbones of two Gly residues of the GY/FG selectivity sequence were mutated, indicating that conformational changes of this invariant sequence affected channel gating and permeation (*19*). Furthermore, Kir2.1-Kir1.2 chimeric channels have shown that the M1-M2 linker of Kirs is an important determinant of channel kinetics (*16*) and that channel open time duration of Kir2.1 depended on Tyr145 of the invariant GY/FG sequence (*17*). These studies support that minor changes in the M1-M2 linker can result in alterations of pore conformations and, therefore, suggest that this linker may be involved in allosteric interactions for regulating transitions of the homomultimeric channel.

Previously, we showed that these Kir2.1 mutants were glycosylated and at the cell surface, suggesting that the putative pore-forming segment of the M1-M2 linker is extracellular (*1*). All the mutants expressed strong inwardly rectifying whole cell currents that were blocked by barium. In addition, we showed that the single channel current amplitudes of Q140N, I143N/Y145S, and F147N/C149T were reduced. In this study, we have shown that the smaller unitary conductances detected in Q140N, I143N/Y145S, and F147N/C149T are also observed in WT Kir2.1 and S128N. Furthermore, the main open unitary conductance of WT Kir2.1 and S128N channels was observed in I143N/Y145T channels. These results indicate that the reductions in the single channel conductances are different intermediate pore conformations of WT Kir2.1 and that the structural changes in the pore are minor. The subtle pore change of the mutant channels suggests that the proteins are folding correctly and that the mutations are not direct structural changes of the pore. Therefore, this study further substantiates our previously proposed topological model that the M1-M2 linker,

including the putative pore-forming segment, is extracellular (*1*, *6*, *7*). We conclude that the extracellular M1-M2 loop is a critical structural determinant in regulating the transitions of the Kir2.1 channel.

ACKNOWLEDGMENT

We thank Dr. Brian D. Cain for comments of the manuscript and Alicia Rudin for excellent technical assistance of this work.

REFERENCES

1. Schwalbe, R. A., Rudin, A., Xia, S.-L., and Wingo, C. S. (2002) *J. Biol. Chem. 277*, 24382−24389.
2. Kubo, Y., Baldwin, T. J., Jan, Y. N., and Jan, L. Y. (1993) *Nature 362*, 127−133.
3. Nichols, C. G., and Lopatin, A. N. (1997) *Annu. Rev. Physiol. 59*, 171−191.
4. Zaritsky, J. J., Redell, J. B., Tempel, B. L., and Schwarz, T. L. (2001) *J. Physiol. 5333*, 697−710.
5. Ho, K., Nichols, C. G., Lederer, W. J., Lytton, J., Vassilev, P. M., Kanazirska, M. V., and Hebert, S. C. (1993) *Nature 362*, 31−38.
6. Schwalbe, R. A., Wang, Z., Bianchi, L., and Brown, A. M. (1996) *J. Biol. Chem. 271*, 24201−24206.
7. Schwalbe, R. A., Bianchi, L., and Brown, A. M. (1997) *J. Biol. Chem. 272*, 25217−25223.
8. Glowatzki, E., Fakler, G., Brandle, U., Rexhausen, U., Zenner, H.-P., Ruppersberg, J. P., and Fakler, B. (1995) *Proc. R. Soc. London, Ser. B 261*, 251−261.
9. Yang, J., Jan, Y. N., and Jan, L. Y. (1995) *Neuron 15*, 1441−1447.
10. Clement, J. P., IV, Kunjilwar, K., Gonzalez, G., Schwanstecher M., Panten, U., Aguilar-Bryan, L., and Bryan, J. (1997) *Neuron 18*, 827−838.
11. Shyng, S.-L., and Nichols, C. G. (1997) *J. Gen. Physiol. 110*, 655−664.
12. Eisenberg, R. S. (1990) *J. Membr. Biol. 115*, 1−12.
13. Fox, J. A. (1987) *J. Membr. Biol. 97*, 1−8.
14. Chapman, M. L., VanDongen, H. M. A., and VanDongen, A. M. J. (1997) *Biophys. J. 72*, 708−719.
15. Sakmann, B., and Trube, G. (1984) *J. Physiol. 347*, 641−657.
16. Choe, H., Palmer, L. G., and Sackin, H. (1999) *Biophys. J. 76*, 1988−2003.
17. So, I., Ashmole, I., Davies, N. W., Sutcliffe, M. J., and Stanfield, P. R. (2001) *J. Physiol. 531*, 37−50.
18. MacGregor, G. G., Xu, J. Z., McNicholas, C. M., Giebisch, G., and Hebert, S. C. (1998) *Am. J. Physiol. 275*, F415−F422.
19. Lu, T., Ting, A. Y., Mainland, J., Jan, L. Y., Schultz, P. G., and Yang, J. (2001) *Nat. Neurosci. 4*, 239−246.
20. Picone, A., Keung, E., and Timpe, L. C. (2001) *Biophys. J. 81*, 2035−2049.
21. Sambrook, J., Fritsch, E. F., and Maniatis, T. (1992) *Molecular Cloning: A Laboratory Manual*, Cold Spring Harbor Laboratory, Cold Spring Harbor, NY.
22. Koster, J. C., Bentle, K. A., Nichols, C. G., and Ho, K. (1998) *Biophys. J. 74*, 1821−1829.
23. Schwalbe, R. A., Wang, Z., Wible, B. A., and Brown, A. M. (1995) *J. Biol. Chem. 270*, 15336−15340.
24. Repunte, V. P., Nakamura, H., Fujita, A., Horio, Y., Findlay, I., Pott, L., and Kurachi, Y. (1999) *EMBO J. 18*, 3317−3324.

BI026304A